Physica A 608 (2022) 128278

Contents lists available at ScienceDirect

Physica A

journal homepage: www.elsevier.com/locate/physa

Nanofacet-density scaling on zig-zag carbon nanotubes within the kinetic 5-vertex growth model

S.I.V. Hontinfinde [a], J. Kple [b,c], T.D. Oke [c], F. Zounmenou [b], J. Adda [a], F. Hontinfinde [b,c,*]

[a] ENSGMM, Université d'Abomey, Benin
[b] Département de Physique, FAST, Université d'Abomey-Calavi, Benin
[c] IMSP Dangbo, Université d'Abomey-Calavi, Benin

ARTICLE INFO

Article history:
Received 18 August 2022
Received in revised form 20 October 2022
Available online xxxx

Keywords:
Zig-zag carbon nanotube
Kinetic 5-vertex model
Monte Carlo simulations
Nanofacet density
Power-law behavior

ABSTRACT

Nanofacets density at the edge of a growing zig-zag single-walled carbon nanotube is investigated by means of a kinetic 5-vertex model. The model comprises, carbon atoms deposition and diffusion events that are assumed Markov processes. The nanotube synthesis temperature, the carbon atomic flux from the catalyst nanoparticles, and the diffusion length are the model physical parameters considered. The kinetic equation describing the nanotube growth is solved by Kinetic Monte Carlo simulations and the average nanofacet density at the nanotube edge is calculated. It is found that this quantity displays interesting behaviors, in particular a power-law behavior with the diffusion length and the growth time.

© 2022 Elsevier B.V. All rights reserved.

1. Introduction

Due to their exceptional properties and technological applications [1–6], single-walled (SW) carbon nanotubes (CNT) attracted much interest in the past three decades. They are key materials for nanoscale photonic and optoelectronic devices [7–9] and are characterized by the chiral angle θ between the tube edge and the zig-zag motif of carbon atoms. Depending on this chirality, their electronic structure can be metallic or semiconducting. However, the incomplete knowledge of atomic scale SWCNT's growth mechanisms greatly hinders SWCNT chirality-selective synthesis in growth experiments. CNTs growth often proceeds via chemical vapor deposition (CVD) [10,11] with metal nanoparticles as catalysts. Theoretically, several growth models were proposed along with screw dislocations and studied [12–14]. In the dislocation theory of CNT growth, any chiral nanotube with conventional indices (n,m) can be viewed as a basic zig-zag tube with a screw dislocation of Burgers vector **b** along its axis [12]. Some of them revealed that the CNT elongation rate is proportional to the Burgers vector, i.e. to the chiral angle of the nanotube [12].

The formation mechanism of carbon nanotubes in CVD experiments is quite complicated. When the chiral angle is selected, one can study in a simplified model with "clean" tube end-rim, incorporation processes of carbon atoms into the nanotube's edge from a gaseous phase and evaluate the tube elongation rate. In this perspective, the growth kinetics of an achiral SWCNT with zig-zag rim has been recently studied by means of a kinetic 5-vertex model [15]. Exact results were provided for small-size versions of the model and larger sizes have been investigated by kinetic Monte Carlo (KMC) simulations using the Bortz–Kalos–Lebowitz (BKL) method [16]. The results achieved indicated that growth can proceed

* Corresponding author at: Département de Physique, FAST, Université d'Abomey-Calavi, Benin.
E-mail address: fhontinfinde@yahoo.fr (F. Hontinfinde).

https://doi.org/10.1016/j.physa.2022.128278
0378-4371/© 2022 Elsevier B.V. All rights reserved.

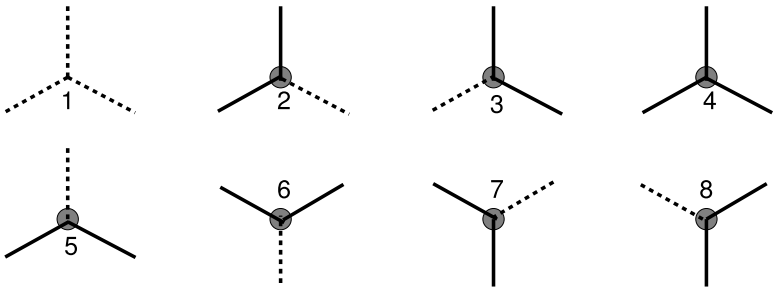

Fig. 1. Schematic line representation of the 8-vertex model.

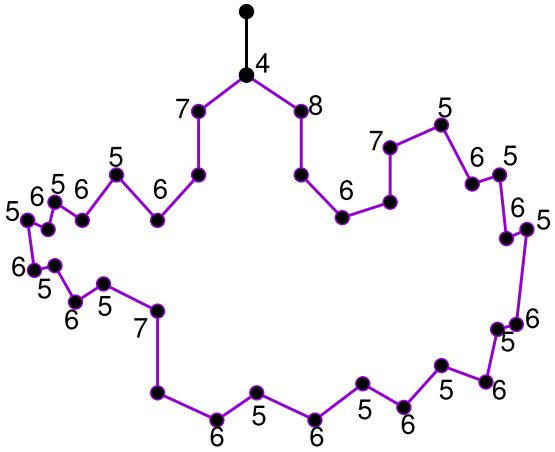

Fig. 2. (color online) Mapping of a SWCNT growing edge of length $L = 30$ with conventional indices (15,2) onto the 5-vertex model. In the description, full vertex lines are used while dashed ones are omitted [15,17].

in a ring-by-ring (layer-by-layer) mode or in a pure continuous mode depending on values of model parameters. More recently, the previous model has been extended to include carbon atoms migration processes at the SWCNT edge [17]. The authors found that in suitable growth conditions, the elongation rate of the nanotube is proportional to its chiral angle θ up to a critical value θ_c that depends on physical parameters. These results are consistent with previous findings from experimental and theoretical works [10–12,14].

In the present study, the previous vertex model with carbon atoms migration is modified [17]. The aim is to derive some CNT edge properties in molecular beam epitaxy conditions often adopted for crystal surfaces growth. Hence, a constant deposition flux F which does not depend explicitly on the temperature is used. By turning values of external parameters, the interplay among deposition and atom diffusion processes on the growing CNT edge leads to the development of some defects and nanostructures at the edge. Therefore, it will be possible to choose model parameters in some well-defined ranges to only activate some specific atomic mechanisms in view to achieve a control of the CNT edge morphology. In this work, we essentially look for the occurrence of nanofacets with conventional indices (n,1), (n,n-1) and (n,n) on the CNT edge and compute their density and scaling behavior with the number of deposited carbon atoms at selected atomic fluxes. An example of such faceting of growing surfaces has been reported on missing-row (110) surfaces in Ref. [18].

The paper is organized as follows. In Section 2, the kinetic 5-vertex model is presented. Section 3 briefly describes the numerical simulation method. Section 4 is devoted to results and discussion. The last section contains concluding remarks.

2. Kinetic 5-vertex model for SWCNT growth

A line representation of the 8-vertex model is depicted in Fig. 1. For the study of the CNT growth kinetics, only vertices 4,5,6,7,8 are relevant [15,17]. In Fig. 2, the edge of a chiral SWCNT with conventional indices (15,2) in the dislocation theory of Ding et al. [12] is mapped onto the 5-vertex model [15,17]. Vertex energies are defined assuming that the CNT with zigzag edge mapped only with vertices 5 and 6 (chirality $c = 0$) should have the minimum energy zero. Other vertices that appear during the edge fluctuations, would be assigned more energy. Hence, vertex energies are considered as follows: $\epsilon_5 = \epsilon_6 = 0$; $\epsilon_4 = \epsilon_7 = \epsilon_8 = \epsilon$. The exact solution of this kinetic 5-vertex growth model uses the technique of transition matrix method described in several previous works [15,17,19–22].

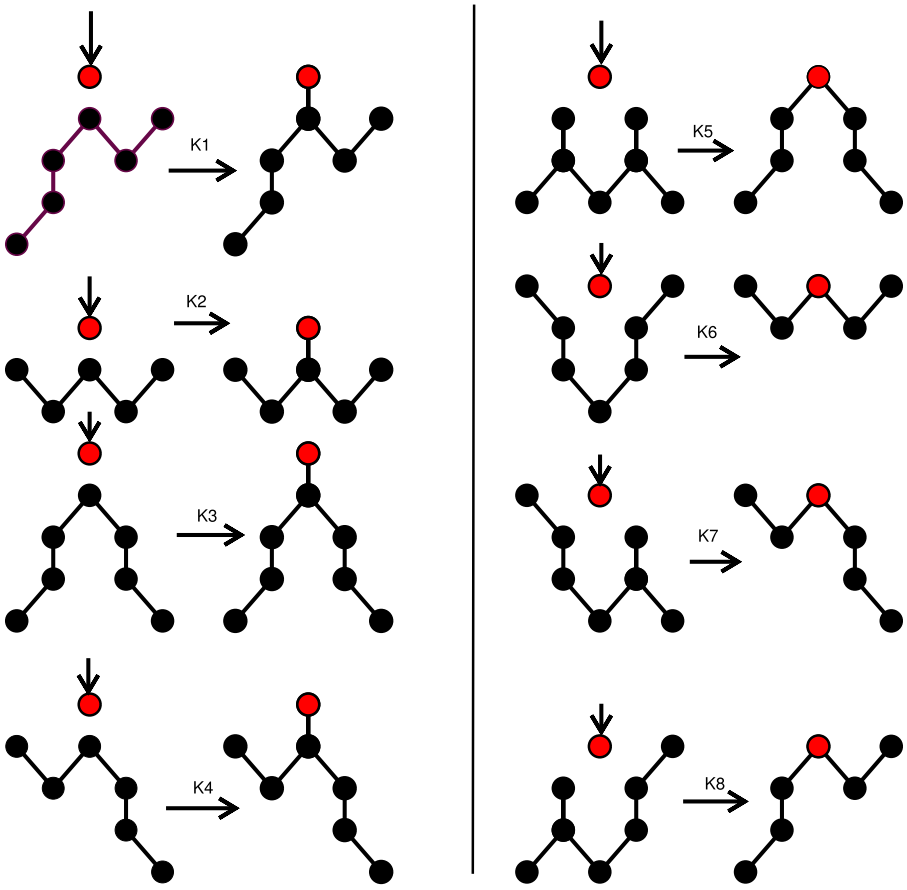

Fig. 3. (color online) Schematic representations of the eight deposition events on the nanotube rim (see text) and associated rim local morphological changes.

A deposition site at the CNT rim is characterized by a 5-vertex subconfiguration formed by three vertices that we termed growth kink subconfigurations (growth active sites). Eight such kinks are found in the model:

$$K_1 = 856, \quad K_2 = 656, \quad K_3 = 857, \quad K_4 = 657,$$
$$K_5 = 464, \quad K_6 = 768, \quad K_7 = 764, \quad K_8 = 468.$$

A diffusion site at the CNT growing edge is characterized by a 5-vertex subconfiguration formed by four vertices that we termed diffusion kinks. We also have 8 different types of these kinks:

$$\overline{K}_1 = 4656, \quad \overline{K}_2 = 4657, \quad \overline{K}_3 = 4764, \quad \overline{K}_4 = 4768,$$
$$\overline{K}_5 = 6564, \quad \overline{K}_6 = 8564, \quad \overline{K}_7 = 4684, \quad \overline{K}_8 = 7684.$$

The four former kinks $\overline{K}$ are diffusion kinks to the right while the latters which are the vertical mirror images of the formers are diffusion kinks to the left.

The dynamics is introduced in the model by carbon atom attachments (Fig. 3) and migrations (Fig. 4) at the CNT edge. The CNT growth results from these two competing processes occurring at different time scales: disordering through carbon atoms deposition at the CNT edge at flux F and ordering through carbon adatoms migration at a hopping rate given by the conventional Arrhenius ansatz: $D = D_0 exp(-\beta E_0)$ where D_0 denotes the attempt frequency and E_0 the hopping energy barrier, $\beta = 1/k_B T$ is the inverse synthesis temperature, k_B is the Boltzmann constant set to 1 in the following.

The constant atomic flux F in the present vertex model is a key parameter expressed in atoms (or monolayers) per unit time. One can study its influence on the growth kinetics and the CNT edge morphology. Such an investigation, has been performed in several numerical simulations for epitaxial growth of metal on metal surfaces, in particular in the submonolayer deposition regime [18,23–25].

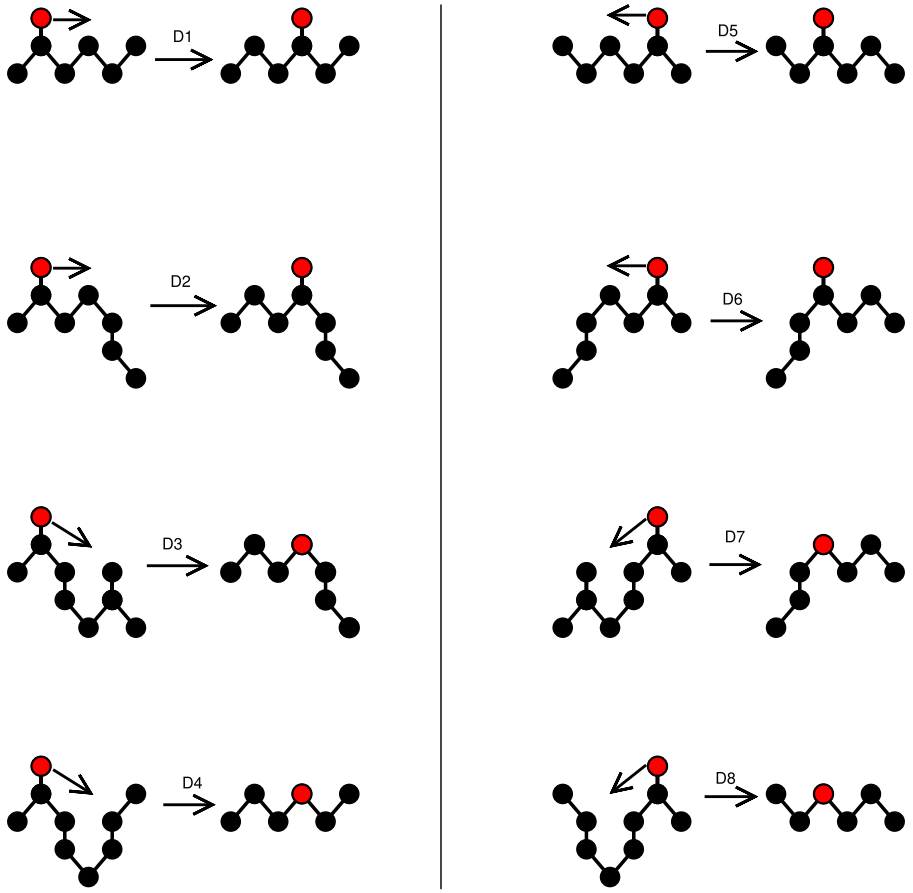

Fig. 4. (color online) Schematic representations of the eight migration processes allowed on the nanotube edge (see text) and associated edge local morphological changes.

The CNT edge relaxation occurs in the model by carbon adatoms migration processes which events are considered as Markov processes that occur at the following rate [17]:

$$D = D_0 \frac{exp(-\beta E_0)}{1 + exp(\beta \Delta E)}, \tag{2.1}$$

where ΔE is the change of the 5-vertex energy of the tube edge when the attempted move is realized; D_0 is the attempted frequency that is assumed to weakly depend on the temperature. In the following, it will be taken proportional to the typical vibration frequency of an isolated carbon adatom on the CNT edge. $D_0 \simeq kT/h$ [17,26] where h is the Planck constant (hereafter set to 1); E_0 is the activation energy that is assumed to be a constant set to ϵ for all diffusive motions. In this formulation, it appears evident that the diffusion process is activated by the change of the environment of the diffusion kink during the diffusive motion due to the presence of ΔE. Denoting $v = \exp(\epsilon/T)$, associated rates are summarized as follows:

$$D_1 = D_2 = D_5 = D_6 = D_0 \frac{1}{2v}, \qquad D_3 = D_7 = D_0 \frac{1}{v + v^{-1}}, \qquad D_4 = D_8 = D_0 \frac{1}{v + v^{-2}}$$

In the model, a new parameter Γ is defined through the relation: $\Gamma = D_1/F$. The deposition rate is taken identical for all growth kinks. As this parameter increases, landing particles can on average travel further between two deposition processes at the CNT edge. Hence, it stands as a measure of the diffusion length of a landing carbon atom at the CNT edge. Physical quantities of interest, as the growth rate, nanofacet densities and the CNT 5-vertex energy will be evaluated as functions of the growth time t (or in the steady state) related to the number N of deposited carbon atoms, the diffusion length Γ and the synthesis temperature T. The latter will be fixed to $T = 10$ for most calculations on nanofacet densities.

3. Kinetic Monte Carlo simulations

Carbon atoms are deposited at the CNT edge at active growth kinks with the above-defined atomic flux. The kinetic Monte Carlo simulations with the Bortz, Kalos and Lebowitz (BKL) algorithm is adopted [16,19–22,26]. In the BKL scheme,

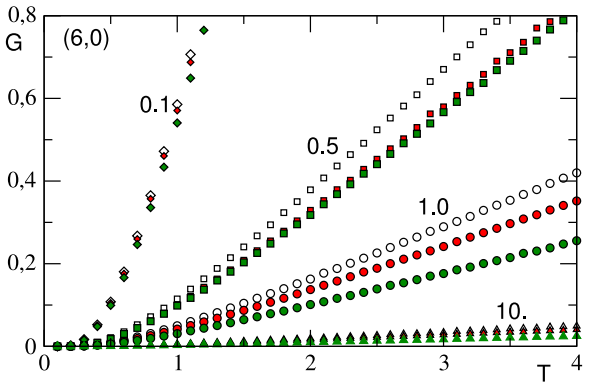

Fig. 5. (color online) Simulated stationary growth rates per site versus temperature T for selected values Γ written on the curves. Three systems with conventional indices (6,0) (open signs), (10,0) (full red signs) and (30,0) (full green signs) are considered. It could be observed that some finite-size effects are present at low values of Γ while at high values, they are weak. At fixed values of Γ, G is an increasing function of the temperature T.

a move is performed at each step according to its a priory probability. For a CNT edge 5-vertex configuration (V) obtained at a given stage of the growth with Ω possible processes and transition rates $T_n,\ n = 1, \Omega$, the total evolution rate R of (V) is the sum of transition rates of all possible events on (V). The real life-time of (V) is given by:

$$\tau = -Log(\bar{r})/R \tag{3.1}$$

where $\bar{r}$ is a random number generated between 0 and 1. The simulations are propagated as follows. A random number r_1 is selected and a random rate $Q = r_1 \times R$ is calculated. By summing rates of updated processes of configuration (V), the first process such that the condition

$$\sum_{n=1} T_n \geq Q \tag{3.2}$$

holds is realized. Then possible processes of the new 5-vertex configuration are updated and the total evolution rate recalculated. After a sufficient simulation time period t where g new configurations have been generated, the values of physical quantities are estimated by a time-averaging procedure. The simulated growth rate G at the steady state is evaluated as follows [19]:

$$G = t^{-1}L^{-1}\sum_{n=1}^{g}\tau(V_n)R(V_n) \tag{3.3}$$

where L denotes the circumference of the CNT or the number of vertices needed in the CNT edge mapping.

4. Results and discussion

The exact solution of the kinetic 5-vertex model with edge diffusion for CNTs growth has been provided in Ref. [17] and a perfect agreement between exact and numerical simulation results was shown. Results presented here have been averaged over 10^3 to 10^4 independent runs. In this section, we mainly focused our attention on the dynamics of nanofacets formation and decay at the CNT edge. In Fig. 5, we displayed simulated values of the elongation rate (in the steady state) for three zig-zag CNTs at selected values of Γ. The system sizes considered are: $L = 12; 20; 60$ which correspond to three systems with conventional indices (6,0), (10,0) and (30,0) (see [12]). We observed first that in the Γ-range studied, G depends on L, i.e., on the diameter b of the CNTs, being a decreasing function of the latter for selected values of physical parameters. The b-dependence of the elongation rate has been also reported in the dislocation theory for chiral CNTs growth of Ding et al. [12]. Other calculations have shown however that in the absence of atoms migration, saturation of G rapidly occurs with increasing L. Second, the synthesis temperature T (expressed in units of ϵ) has a major effect on G. G increases with T at fixed values of Γ. This appears physical since, an increase of T enhances carbon atoms migration processes which should speed up the tube elongation process.

Simulation data are influenced by the CNT 5-vertex energy E due to the dependence of diffusion events on the latter. In a ring-by-ring growth, the energy may be close to zero. In unstable growth dominated by atoms migration processes, it should be high due to the appearance of large local slopes at the edge in multilayer growth. In Fig. 6, the behavior of E in the early stage of the growth is illustrated at three different temperatures for selected values of Γ. It results that a non-monotonic behavior of E versus growth time t is observed in all panels. E increases sharply when about L/2 atoms are deposited and this happens at all selected temperatures. For low values of Γ, the early growth stage total deposition

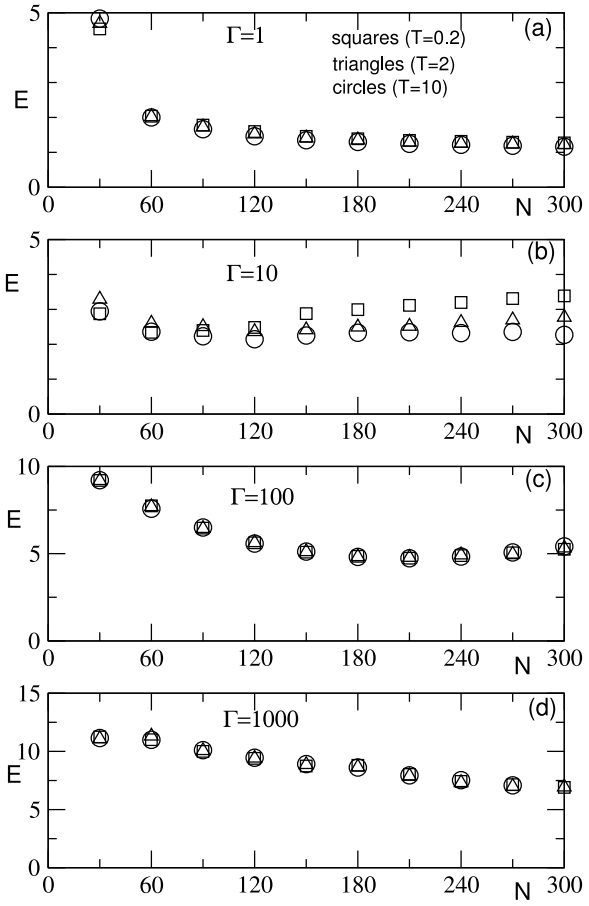

Fig. 6. Behavior of the (30,0)-CNT 5-vertex energy E as a function of the growth time $N = F \times t$ at three selected temperatures: $T = 0.2$; 2.0; 10.0. E increases at the beginning of the CNT growth, passes by a maximum and then decreases. It tends to oscillate in some cases, in particular for large values of Γ. In some model parameters ranges, E does not significantly change with T.

rates may exceed the total diffusion rates at the edge and a deposition process is often selected. Then the increase of the 5-vertex energy E results from the proliferation of carbon adatoms at the CNT edge. The complete formation of one layer needs a 60 atoms deposition. Due to the smoothing character of migration processes, the energy E should decrease as observed. It is evidenced that at $\Gamma = 10$, the effect of the temperature T is remarkable with E decreasing with increasing values of T.

In crystals growth, several studies have been performed on island-size density and scaling in deposition processes (see [27] and references therein), in particular in the submonolayer regime. Applying crystals growth concepts to CNTs growth, we found instructive to study formation and decay of nanostructures at the edge of a growing CNT. In a previous work on zig-zag CNTs growth, the dynamical development of some nanofacets has been illustrated and their formation energies calculated [15]. Such a dynamical faceting has been also reported in Ref. [18]. In this work, instead of studying hexagon islands density at the CNT edge, we investigated the dynamics of nanofacets formation and studied the behavior of their density with the diffusion length Γ and growth time t measured by the number N of carbon atoms added to the CNT edge at fixed values of Γ. The nanofacet density f is defined as $f = d/L$, where d is the calculated average number of nanofacets at the nanotube rim at a given simulation time. Since L which denotes the nanotube rim size is a constant, the quantity d will be considered in the following as the nanofacet density. Nanofacets with conventional indices (n,1), (n,n-1), and (n,n) are those considered in the investigation and the temperature in all calculations was set to $T = 10$. A schematic representation of some nanofacets of the family (3,m) is depicted in Fig. 7 where two different vertex configurations of (3,2) and (3,3) nanofacets were shown. The average number of nanofacets of each type is calculated at every deposition of 60 carbon atoms at the CNT edge. It is observed from Fig. 8a that for $\Gamma = 10$, the nanofacet average densities present a non-monotonic behavior. They increase in the early growth regime, then pass by a maximum and later decrease. It is worthwhile to focus on this decrease regime of nanofacets density. In Fig. 8b, a log–log plot of the density d as a function of N is depicted for different nanofacets densities illustrated in Fig. 8a. There, the linear behavior of simulated data is evident. It results that a power-law behavior of the nanofacet density is got as observed in Ref. [27]

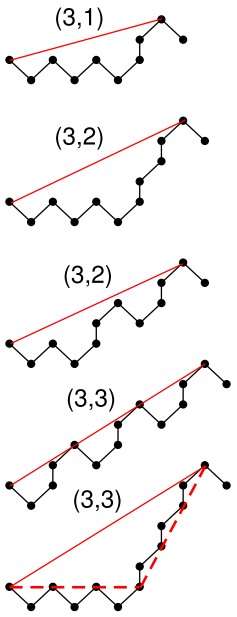

Fig. 7. (color online) Schematic representations of some nanofacet configurations of conventional indices (3,m) locally observed at the edge of a growing zig-zag carbon nanotube.

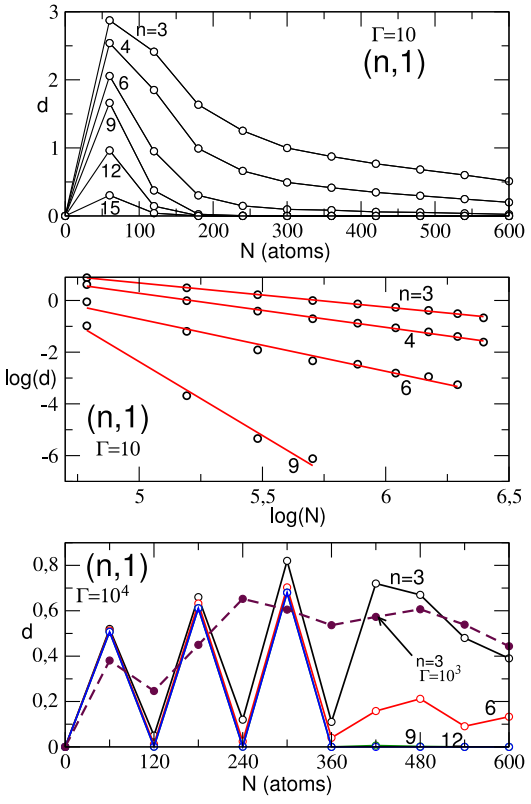

Fig. 8. (color online) KMC simulated nanofacet (n,1) densities as function of growth time $N = F \times t$ for $\Gamma = 10$ (panels a,b) and $\Gamma = 10^3,\ 10^4$ on a (30,0)-CNT growing edge. d increases, passes by a maximum and then decreases (panel a). A log–log plot of these densities in the decreasing region is performed in panel b. A linear behavior of data appears evident, suggesting the existence of a power-law scaling of the nanofacet densities with growth time. For $\Gamma = 10^4$ (panel c), periodic oscillations are observed in the early stage of the CNT growth. All (n,1) nanofacets show the same oscillations period of 120 atoms. The behavior looks different for $\Gamma = 10^3$ (panel c).

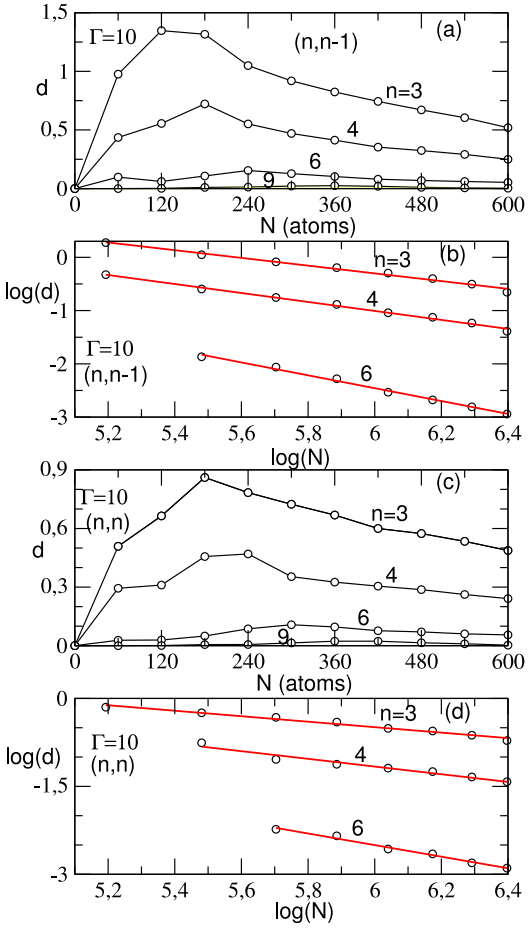

Fig. 9. (color online) KMC simulated nanofacet (n,n-1) and (n,n) densities as functions of growth time $N = F \times t$ for $\Gamma = 10$ (panels a,c) on a (30,0)-CNT growing edge. d increases, passes by a maximum and then decreases. A log–log plot of these densities in the decreasing region is performed in panels b and d. A linear behavior of data is observed, suggesting the existence of a power-law scaling of nanofacet densities with growth time.

concerning island-size density with growth time. Nanofacets are different from islands but surprisingly both densities have shown the same power-law behavior with the diffusion length. There is here, however, a difference with respect to observations of Ref. [27]. In the latter, the scaling has been detected in the submonolayer regime while in the present investigation, it appears after several monolayers have been deposited. Since $N = F \times t$, one can write this behavior in the form: $d \sim (Ft)^{-\gamma}$, where γ is the time-exponent obtained by a linear regression procedure. Our calculations yielded the following values of γ: 0.93087 ± 0.018 for (3,1) nanofacet; 1.317 ± 0.033 for (4,1) nanofacet; 2.022 ± 0.012 for (6,1) nanofacet; 5.709 ± 0.460 for nanofacet (9,1). One remarks that the exponent γ is increasing with the nanofacet length. Further, the parameter Γ is increased to 10^4 in Fig. 8c. There, one observes that the behavior is completely different from the previous one in this diffusion-dominated regime. In epitaxial growth of metal on metal surfaces for thin films deposition, larger values of Γ, about $\Gamma = 10^6$, are used. In this panel, two different regimes can be identified. In the first regime which corresponds to the early stage of the growth process, a kind of oscillation of the density with increasing amplitude is observed. The period of the oscillations is constant about $N = 120$ atoms for all nanofacets at this value of Γ. These oscillations indicated that the ring roughness also oscillates as in a ring-by-ring growth mode. For $\Gamma = 10^3$, the behavior is quite different as shown in the same panel for (3,1) nanofacet. In the second regime that starts around $N = 420$, damping oscillations become evident with possibly a final decrease as in panel (a). Concerning systems (n,n-1), calculations yielded results displayed in Fig. 9a while for (n,n) nanofacets, results are shown in Fig. 9c. They look similar compared to those reported in Fig. 8a for $\Gamma = 10$. Following exponents have been derived from log–log plots of d in the decreasing parts of different d-curves: 0.725 ± 0.034 for nanofacet (3,2); 0.841 ± 0.025 for (4,3); 1.208 ± 0.041 for (6,5); 5.154 ± 0.250 for (9,8). For systems (n,n), we got: 0.466 ± 0.027 for (3,3); 0.655 ± 0.060 (4,4); 0.988 ± 0.054 for (6,6). Values of γ decrease with the nanofacet length. The power-law behavior is also obtained for $\Gamma = 100$ at the same

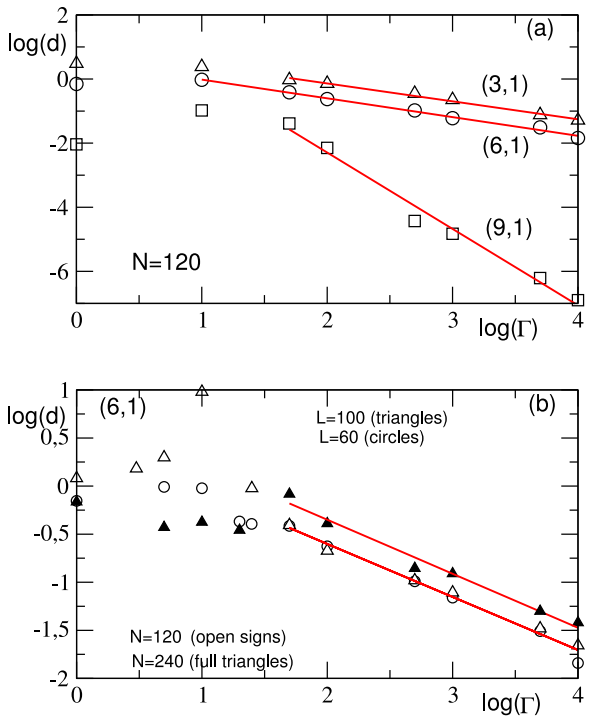

Fig. 10. (color online) Log–log plots of nanofacets (n,1) densities as functions of Γ at fixed growth times for a (30,0)-CNT rim. In each case, a Γ-region is found for the existence of the power-law behavior $d \sim \Gamma^{-\alpha}$. Panel b shows that almost the same exponent α is obtained for two system sizes $L = 60$ and $L = 100$ at two different growth times $N = 120$ and $N = 240$ atoms.

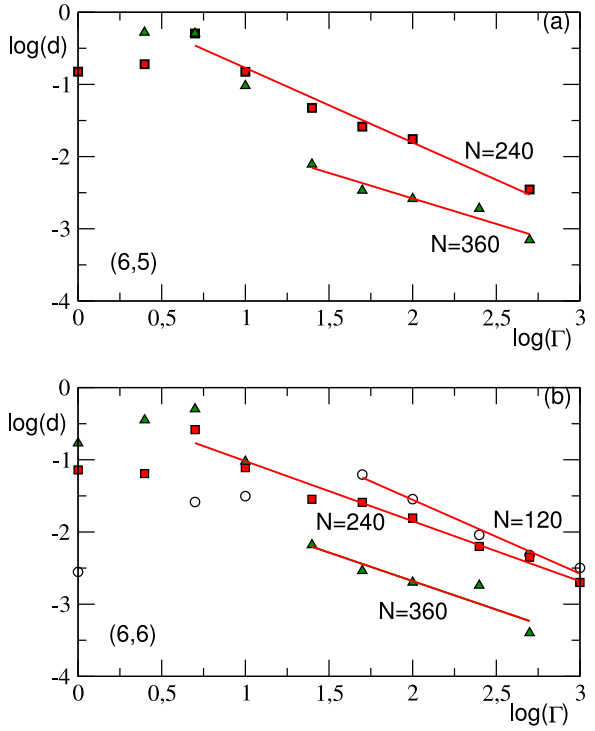

Fig. 11. (color online) Log–log plots of nanofacets (6,5) (panel a) and (6,6) (panel b) densities as functions of Γ at fixed growth times for a (30,0)-CNT rim. In each case, a Γ-region is found for the existence of the power-law behavior $d \sim \Gamma^{-\alpha}$. The best results are obtained for $N = 240$ atoms.

temperature. It is important to stress that in the submonolayer regime, we checked that this scaling is completely absent. It only appears after a certain number of atomic layers has been deposited. This number increases with increasing values of n.

It is worthwhile to investigate the behavior of densities d with the parameter Γ at selected values of the growth time t i.e., when well-defined numbers of carbon atomic layers have been deposited. In Fig. 10a, $log(d)$ versus $log(\Gamma)$ is plotted for (3,1), (6,1) and (9,1) nanofacets for $N = 120$ atoms. We found a domain of Γ (diffusion-dominated regime) where the relation: $d \sim \Gamma^{-\alpha}$ holds. While for (3,1) and (6,1) nanofacets, α almost has the same value, it sharply increases for (9,1). This change of behavior may be due to the length of (9,1) nanofacet. More calculations are certainly needed to clarify this finding. On the other hand, Fig. 10b brings to our notice other crucial informations. Indeed, there, finite-size effects on previous results are investigated. At $N = 120$, CNTs with $L = 100$ and $L = 60$ yielded almost the same density at high values of Γ whereas at low values, finite-size effects are important. It is also evidenced that at large values of Γ and two different growth times, densities for $L = 60$ and $L = 100$ are different but they almost show the same scaling behavior as regression lines are almost parallel.

In Fig. 11, nanofacets (6,5) and (6,6) are investigated at some selected growth times: $N = 120$; 240; 360 atoms. From log–log plots of densities as functions of Γ for a (30,0)-CNT rim, it is evidenced that a Γ-range does exist for each plot where a power-law behavior $d \sim \Gamma^{-\alpha}$ prevails. Results appear interesting for $N = 240$ atoms. There, a wide Γ-region is got for this scaling. We found for (6,5)-nanofacet, $\alpha = 1.033$ for $N = 240$ atoms and $\alpha = 0.705$ for $N = 360$ atoms. In the case of (6,6)-nanofacet, we obtained $\alpha = 0.83$ for $N = 240$ atoms and $\alpha = 0.79$ for $N = 360$ atoms.

From results displayed above, one can write the nanofacet density in the following form: $d \sim (Ft)^{-\gamma} \times (D/F)^{-\alpha}$. This general scaling is similar to the one obtained in Ref. [27] for island-size density. The appearance of nanofacets on the growing edge is limited by hexagons and mounds formation at this edge. When an hexagon is nucleated on the zig-zag edge, this gives rise to the birth of nanofacets of (n,1) kind. When mounds are nucleated due to large values of Γ (fast diffusion processes), the probability of nucleation of (n,n-1)- and (n,n)-nanofacets is enhanced due to an increase of growth instability in multilayer deposition context.

5. Conclusion

The study of carbon nanotubes becomes a hot topic that attracts even the general public beyond scientists and industrials. This motivated the present work where a kinetic 5-vertex model is used to study the dynamics of nanofacets formation on growing zigzag carbon nanotubes. The basic issues were the determination of the non-equilibrium scaling behavior of these nanofacet densities in the early stage of the tube growth process with system parameters, in particular the diffusion length (measured by the ratio of diffusion rate to the deposition rate) and growth time. Our calculations yielded interesting results. Indeed, a power-law of nanofacets density scaling with the diffusion length Γ and also with the growth time t is discovered. This finding suggested a behavior of the density of the form: $d \sim (F.t)^{-\gamma} \times \Gamma^{-\alpha}$. Similar scaling behavior has been reported in Ref. [27] on island-size density in deposition processes on crystal surfaces. The results are quite surprising since nanofacets density is not explicitly correlated to carbon atom islands at the growing edge. The origin of this scaling behavior needs to be elucidated by more numerical investigations. One question needs to be also elucidated. It concerns the chirality distribution of CNTs with well-defined indices in growth experiments. We need to know whether there exists a correlation between this distribution with results on nanofacets density on zig-zag nanotubes displayed in the present work. Moreover, it is worth noting that the study of the effect of the tube chirality on the nanofacets density would be very interesting. It will be checked whether the power-law scaling reported in the present work, exists. Work on the subject is in progress.

Declaration of competing interest

The authors declare that they have no known competing financial interests or personal relationships that could have appeared to influence the work reported in this paper.

Data availability

No data was used for the research described in the article.

References

[1] R.H. Baughman, A.A. Zakhidov, W.A. de Heer, Carbon nanotubes—The route toward applications, Science 297 (2002) 787–792.
[2] M. Vahdani Moghaddam, P. Yaghoobi, G.A. Sawatzky, A. Nojeh, ACS Nano. 9 (2015) 4064.
[3] N. Perea-Lopez, B. Rebollo-Plata, J.A. Briones-Leon, A. Morelos-Gomez, D. Hernandez-Cruz, G.A. Hirata, et al., ACS Nano. 5 (2011) 5072.
[4] L.V. Titova, C.L. Pint, Q. Zhang, R.H. Hauge, J. Kono, F.A. Hegmann, Nano Lett. 15 (2015) 3267.
[5] X. He, N. Fujimura, J.M. Lloyd, K.J. Erickson, A.A. Talin, Q. Zhang, et al., Nano Lett. 14 (2014) 3953.
[6] J.H. Taphouse, O.N.L. Smith, S.R. Marder, B.A. Cola, Adv. Funct. Mater. 24 (2014) 465.
[7] N. Chiodarelli, Y. Li, D.J. Cott, S. Mertens, N. Peys, M. Heyns, et al., Microelectron Eng. 88 (2011) 837.
[8] R. Xie, C. Zhang, M.H. van der Veen, K. Arstila, T. Hantschel, B. Chen, et al., Nanotechnology 24 (2013) 125603.
[9] E. Theocharous, C.J. Chunnilall, R. Mole, D. Gibbs, N. Fox, N. Shang, et al., Opt. Express 22 (2014) 7290.

[10] S.M. Bachilo, L. Balzano, J.E. Herrera, F. Pompeo, D.E. Resasco, R.B. Weisman, J. Am. Chem. Soc. 125 (2003) 11186.
[11] S. Maruyama, Y. Miyauchi, Y. Murakami, S. Chiashi, New J. Phys. 5 (2003) 149.141–149.112.
[12] F. Ding, A.R. Harutyunyan, B.I. Yakobson, Proc. Natl. Acad. Sci. USA 106 (2009) 2506, http://dx.doi.org/10.1073/pnas.0811946106.
[13] V.I. Artyukhov, E.S. Penev, B.I. Yakobson, Nature Commun. 5 (2014) 4892.
[14] M. He, et al., Sci. Adv. 5 (2019) eaav9668, http://dx.doi.org/10.1126/sciadv.aav9668.
[15] F. Zounmenou, R.D. Hontinfinde, F. Hontinfinde, Physica A 594 (2022) 127013.
[16] A.B. Bortz, M.H. Kalos, J.L. Lebowitz, J. Comput. Phys. 17 (1975) 10.
[17] T.D. Oke, S.I.V. Hontinfinde, M. Karimou, F. Zounmenou, F. Hontinfinde, Physica E 142 (2022) 115298.
[18] F. Hontinfinde, A. Videcoq, F. Montalenti, R. Ferrando, Chem. Phys. Lett. 398 (2004) 50.
[19] A.V. Kpadonou, F. Hontinfinde, Physica A 362 (2006) 345.
[20] F. Hontinfinde, M. Touzani, Surf. Sci. 338 (1995) 236.
[21] F. Hontinfinde, R. Ferrando, A.C. Levi, Physica A 319 (2003) 36.
[22] F. Hontinfinde, J. de, Physique I 7 (1997) 767.
[23] R. Ferrando, F. Hontinfinde, A.C. Levi, Phys. Rev. B 56 (1997) 4406.
[24] C. Mottet, R. Ferrando, F. Hontinfinde, A.C. Levi, Surf. Sci. 417 (1998) 220.
[25] F. Hontinfinde, R. Ferrando, Phys. Rev. B 63 (2001) 121403.
[26] F. Hontinfinde, J. Krug, M. Touzani, Physica A 237 (1997) 363.
[27] M.C. Bartelt, M.C. Tringides, J.W. Evans, Phys. Rev. B 47 (1993) 13891.